Results in Optics 16 (2024) 100688

Contents lists available at ScienceDirect

Results in Optics

journal homepage: www.sciencedirect.com/journal/results-in-optics

Invited Article

Web-based application software for Judd-Ofelt analysis of Eu^{3+} ion luminescence

E.H.H. Hasabeldaim *, H.C. Swart, R.E. Kroon *

Department of Physics, University of the Free State, Bloemfontein 9300, South Africa

ARTICLE INFO

Keywords:
Web application
Eu^{3+}
ZnO
Photoluminescence
Judd-Ofelt

ABSTRACT

This article reports on the development of a new Web-based application software for calculating Judd-Ofelt intensity parameters and derived quantities from the emission spectra of Eu^{3+} doped compounds. The application was entirely developed in JavaScript, and it is compatible with all major browsers. The web application can be accessed via the following link https://sciapps.sci-sim.com/judd_ofelt_analysis_Eu.html. Test samples of ZnO doped with different amounts of Eu^{3+} were synthesized using the combustion method, and their radiative properties and the chemical environment in the Eu surroundings were thoroughly investigated by Judd-Ofelt intensity and the derived parameters using the online application. In contrast to the tediousness and time-consuming process of these types of calculations, by using this online software, all intensity parameters and the derived quantities can be obtained within a short time.

1. Introduction

In recent years, rare earth ion (REI) doped materials have received substantial research attention due to their narrow band emission features that permit novel photonic applications (Steckl and Zavada, 1999; Liu and Jacquier, 2006). Among all REIs, trivalent europium (Eu^{3+}) is one of the most investigated ions that has been researched for various modern applications, because of its fascinating luminescent centre owing to its sharp and intense red emission around 617 nm (Shivakumara, 2015). Judd-Ofelt (JO) parameters play a pivotal role in understanding the radiative properties and chemical environment of REIs in hosts. They are usually obtained from absorption spectra (Judd, 1962; Ofelt, 1962). Due to the uniqueness of the Eu^{3+} ion, particularly its magnetic dipole transition which can be used as a reference for other transitions, JO parameters can be obtained from luminescence emission spectra. Another unique feature is that all values of the squared reduced matrix elements ($|\langle J||U^J||J'\rangle|^2$) of the electric dipoles are zero, except the diagonal elements that correspond to the $^5D_0 - {}^7F_J$ (J = 2, 4, and 6) transitions are non-zero and can be computed (Cantelar et al., 2020). Moreover, JO analysis provides useful information, including stimulated emission cross-section, radiative transition probability, optical gain, and branching ratio, as well as other derived parameters (Yu et al., 2019). Thorough understanding of JO parameters and their derived quantities permits material composition optimization and enhanced lasing properties of selected transitions (Danmallam et al., 2019). Furthermore, JO intensity parameters also give information about the structural changes and ligand interactions, including the degree of covalency in the vicinity of REIs, as well as their role in the emission properties (Kumar et al., 2016).

Obtaining the JO intensity and the derived parameters by hand is a tedious and cumbersome process. Therefore, the availability of a suitable computer program to perform these calculations is convenient for researchers. There are a few software applications to accomplish this, but each application has its own downsides. RELIC application software is one of the most commonly used to attain JO intensity parameters, but it requires an absorption spectrum that is three times less sensitive than an emission spectrum, and it implements a complex fitting algorithm to retrieve the parameters (Hehlen et al., 2013; Hehlen, n.d.). Therefore, it is not suitable for a quick evaluation of JO and derived parameters of Eu^{3+} ions from emission spectra. The LUMPAC software package is an available option to compute JO parameters of Eu^{3+} from emission spectra, but it is limited to two intensity parameters and cannot calculate the derived parameters such as the effective bandwidth of the emission transitions, stimulated emission cross-sections, gain bandwidths, and optical gains (Dutra et al., 2014). A simple script using MathCal 14* software has also been introduced as a suitable platform to calculate JO intensity parameters from an emission spectrum, but it is commercial software and is only compatible with Microsoft Windows. Recently,

* Corresponding authors.
E-mail addresses: KroonRE@ufs.ac.za (E.H.H. Hasabeldaim), kroonre@ufs.ac.za (R.E. Kroon).

https://doi.org/10.1016/j.rio.2024.100688
Received 18 January 2024; Received in revised form 10 April 2024; Accepted 12 April 2024
Available online 18 April 2024

Aleksandar Ćirić et al. developed the JOES cross-platform software that is able to calculate the JO parameters of Eu from an emission spectrum but lacks the ability to calculate other important derived parameters (Ćirić et al., 2019).

This work presents a newly developed web-based application for computing JO intensity and derived parameters of Eu^{3+} from an emission spectra. The user needs only the Eu^{3+} emission data file, the refractive index of the host material, and the observed lifetime to obtain the intensity and derived parameters. The user does not need to download or install any software or any dependencies, since the software is accessible through the URL and is compatible with all major web browsers. To illustrate the software, ZnO:Eu test samples were synthesized via the combustion method, and their radiative and lasing properties, as well as the chemical environments in the surrounding area have been thoroughly evaluated.

2. Theory

2.1. Judd-Ofelt parameters

Among all the rare earth (RE) elements, europium (Eu) is exceptional because its magnetic dipole (MD) transition probability is independent of the coordination structure and all of its reduced matrix elements of the electric dipole (ED) facilitated by the $^5D_0$ energy level are zero, except for the transitions that decay to $^7F_\lambda$ where $\lambda = 2$, 4, and 6 (L. ačanin et al., 2011; Görller-Walrand and Binnemans, 1998; Carnall et al., 1989). The line strength of the magnetic dipole is precisely computed and has been used as a reference to obtain Judd-Ofelt parameters for transitions originated from the $^5D_0$ energy level [11]

$$S_{MD} = 9.6 \times 10^{-42} esu^2 (3.2022 \times 10^{-51} C^2)$$

The values of the reduced matrix elements $|\langle J||U^J||J'\rangle|^2$ corresponding to the ^7F_J transitions where J = 2, 4, and 6 have also been calculated as 0.0032, 0.0023, and 0.0002, respectively, and have been used to obtain Judd-Ofelt parameters of Eu^{3+} from photoluminescence spectra (Gökçe et al., 2017). The $^5D_0$ – ^7F_J transitions where J = 0, 3, and 5 are forbidden and therefore not used for calculating Judd-Ofelt parameters. JO intensity parameters Ω_J (J = 2, 4, and 6) can be calculated from the emission spectrum of Eu^{3+} ions in a host material using the following equation (Ilhan et al., 2021)

$$\Omega_J = \frac{S_{MD}(\nu_1^3)}{e^2(\nu_J^3)} \frac{9n^3}{n(n^2+2)^2} \frac{\int I_1(\nu_1)}{|\langle J||U^J||J'\rangle|^2 \int I_J(\nu_J)} \quad (1)$$

where ν_1, ν_J and I_1, I_J represent the frequencies and intensities of the $^7F_1$ and ^7F_J emissions (J = 2, 4, and 6), respectively, e is the elementary charge and has value of 4.803 x 10^{-10} esu

(1.602×10^{-19} C), and n is the refractive index of the material. In the past Ω_2 was usually associated with the ligand symmetry and covalency in the vicinity of the Eu^{3+} ions: a high value of Ω_2 indicates a high degree of Eu^{3+}–O^{2-} covalency bonding and local symmetry distortion, whereas Ω_4 was not directly related to the symmetry but the medium rigidity where Eu^{3+} ions are embedded, and its increased value suggests a lower rigidity or higher viscosity of the surroundings (Tan et al., 2020). However, Moura Jr *et al.* (Moura et al., 2016) have definitively demonstrated that the covalency of the ion-ligand bonding becomes more significant with increasing the Ω_J ranking, which means that Ω_4 and Ω_6 are better probes on quantifying Eu^{3+}-ligand bond covalency than Ω_2.

The spontaneous transition probability is closely related to its electric dipole (ED) and magnetic dipole (MD) strengths and can be computed by Eq. (2) (Ilhan et al., 2021).

$$A(J,J') = \frac{64\pi^4\nu^3}{3h(2J+1)}[\chi_{ED}S_{ED} + \chi_{MD}S_{MD}] \quad (2)$$

Here, J represents the total angular momentum of the initial state and h is Planck's constant. S_{ED}, χ_{ED}, and χ_{MD} are the electric dipole line strength, local field correction of the electric dipole, and the local field correction of the magnetic dipole, respectively which can be found from (Hasabeldaim et al., 2019)

$$S_{ED(J,J')} = e^2\Omega_J|\langle J||U^J||J'\rangle|^2 \quad (3)$$

$$\chi_{ED} = \frac{n(n^2+2)^2}{9} \quad (4)$$

$$\chi_{MD} = n^3 \quad (5)$$

The refractive indexes can be obtained from literature, refractive index database at https://refractiveindex.info/ or calculated by using the following formula (Korotkov and Atuchin, 2008)

$$\frac{n^2-1}{n^2+2}\frac{1}{\rho} = \frac{\sum l_i r_i}{M}$$

where M is the material molar mass, ρ represents the material density, l_i is the atomic number of the material elements, and r_i is the specific refraction of an element. For accurate results, the refractive index corresponding to each wavelength must be given.

The total radiative probability (A_r) can be obtained by summing up the spontaneous transition probabilities of $^5D_0$ – ^7F_J (J = 1, 2, 4, and 6) transitions according to (Babu et al., 2007; Brik et al., 2015)

$$A_r = \sum A(J,J') \quad (6)$$

Branching ratio of Eu^{3+} transitions is useful parameter, especially when the search for a laser emission arise. It can provide valuable information about the material applicability as laser medium. A branching ratio value greater than 50 % indicates that the emission has potential for laser applications (Ćirić et al., 2019; Ilhan et al., 2021). The branching ratio can be calculated by using

$$\beta(\%) = \frac{A(J,J')}{\sum_{J=2,4,6} A(J,J')} \times 100\% \quad (7)$$

2.2. Derived parameters

The observed lifetime (τ) is sum of the radiative (τ_r) and nonradiative (τ_{nr}) lifetimes $\tau = \tau_r + \tau_{nr}$ [18], where the radiative lifetime is the reciprocal of the total radiative probability

$$\tau_r = \frac{1}{A_r} \quad (8)$$

The radiative lifetime is strongly associated with the emission spectrum of Eu^{3+} and can be determined theoretically (Werts et al., 2002)

$$\tau_{cal} = \frac{n^3}{14.65}\frac{I_1}{I_{total}} \quad (9)$$

where τ_{cal} represents the calculated radiative lifetime, n is the host refractive index, I_1 is the integrated intensity of the $^5D_0$ – $^7F_1$ transition, 14.65 (per second) is the value of the spontaneous emission probability for the $^5D_0$ - $^7F_1$ transition in vacuo, and I_{total} is the total integrated intensities of the $^5D_0$ – ^7F_J (J = 1, 2, 4, and 6) transitions (Werts et al., 2002).

The experimental (observed) lifetime (τ) is the time of decaying of the population through radiative (emission) and non-radiative processes, whereas the radiative lifetime (τ_r) is the time that the population would decay at if non-radiative processes did not exist. Quantum yield is the ratio between the number of emitted and absorbed photons, while the quantum efficiency (also known as the intrinsic quantum yield or internal quantum yield) is the ratio between the radiative and the total

rate (Eqs. (11) and (12) (Moura et al., 2016)

$$\eta_{QE} = \frac{\tau}{\tau_r} \tag{11}$$

$$\eta_{QE}^{cal} = \frac{\tau}{\tau_{cal}} \tag{12}$$

Another important derived parameter is the stimulated emission cross-section. It is useful when the need to predict a material's lasing performance arises. The stimulated cross-sections (σ_e) for ^7F_J (J = 1, 2, 4, and 6) having spontaneous transition probability of $A(J, J')$ is given by (Saraf et al., 2015)

$$\sigma_e(\lambda_p)(J, J') = \left[\frac{(\lambda_p)^4}{8\pi c n^2 \Delta\lambda_{eff}}\right] A(J, J') \tag{13}$$

where λ_p is the emission peak wavelength, c is the speed of light, and $\Delta\lambda_{eff}$ represents the effective bandwidth of the transition emission. High values of the stimulated cross-section signify that the material has potential as low threshold and high gain laser material at room temperature. The gain band width $(\sigma_e \times \Delta\lambda_{eff})$ and optical gain $((\sigma_e \times \tau)$ can also be determined and are useful for predicting the gain width of an optical amplifier.

3. Experimental

Three ZnO samples doped with different concentrations of Eu^{3+} ions were synthesized using the combustion method. Zinc nitrate hexahydrate and europium nitrate hydrate were used as zinc and europium sources, respectively, and urea was used as a fuel. 14.95, 14.89, or 14.85 mmol of zinc nitrate hexahydrate were dissolved in 50 ml of deionized water. Next, 0.0495, 0.099, or 0.15 mmol of europium nitrate hydrate was added to the previous solution and stirred for 20 min. Finally, 25 mmol of urea was added to the solution, and the stirring was continued for 30 min. The stock solution was transferred into a ceramic crucible and put in a muffle furnace for 10 min. The resulting powder was ground and annealed at 800 °C for 1 h. A Bruker D8 Advance X-ray diffractometer instrument was used for crystallography measurements. An FS5 fluorescence spectrometer (Edinburgh Instruments) was used for the photoluminescence and lifetime measurements.

4. Results

Fig. 1(a) shows the X-ray powder diffraction patterns of the ZnO doped with different Eu concentrations. The pattern of the ZnO sample doped with 0.33 mol% of Eu ions exhibited peaks that corresponded to planes of the hexagonal wurtzite structure of ZnO (ICSD card no. 29272). The absence of extra peaks associated with Eu compounds suggests an entire incorporation of Eu ions into the ZnO lattice by replacing Zn sites. Fig. 1(b) depicts the Eu ion replacing the Zn site in a hexagonal wurtzite structure of the ZnO lattice. At relatively higher concentrations (0.66 and 1.00 mol%), a small peak marked with an asterisk is present at $2\theta \approx 28.3^\circ$. This peak is assigned to the Eu_2O_3 phase (JCPDS Database no. 43–1009) that formed alongside the ZnO phase.

Fig. 2(a) depicts the photoluminescence spectra of the ZnO phosphors doped with different Eu^{3+} concentrations. The excitation spectra of the samples revealed narrow bands at about 464 nm, 415 nm, and 396 nm ascribed to the $^7F_0 - {}^5D_2$, $^7F_0 - {}^5D_3$, and $^7F_0 - {}^5L_6$ transitions of Eu^{3+}, respectively. In addition, the sample containing 0.33 mol% of Eu ions displayed a broad excitation band centred at about 250 nm due to the Eu-O charge transfer (Hasabeldaim et al., 2019). This band disappeared for the samples with a relatively higher Eu concentration, which could be due to the change of the Eu^{3+} site and the formation of the Eu_2O_3 phase, as revealed by the X-ray powder diffraction analysis. All samples were excited at 464 nm via the $^7F_0 - {}^5D_2$ energy level of Eu^{3+} ion, and the emission spectra exhibited the distinctive Eu^{3+} bands facilitated by the $^5D_2 - {}^7F_J$ (J = 0, 1, 2, 3, and 4) transitions (Hasabeldaim et al., 2020). The sample containing 0.33 mol% of Eu^{3+} ions showed the highest PL intensity with narrow bands. The band that is facilitated by the $^5D_2 - {}^7F_2$ transition was split into two narrow bands, whereas the bands due to $^5D_2 - {}^7F_J$ (J = 1, 3, and 4) transitions have exhibited a shoulder next to the main bands, which indicates the split of these transitions into two bands. This splitting suggests that at relatively low concentrations (0.33 mol%), Eu^{3+} ions have replaced zinc ions in the wurtzite hexagonal structure with C_6/C_{6v} point group symmetry. These features disappeared at relatively higher Eu ion concentrations (0.66 and 1.00 mol%), which suggests a change in the crystal structure and the local chemical environment. These results are consistent with the X-ray powder diffraction analysis. As the Eu^{3+} concentration increased, the PL intensity decreased, and the band width became wider. The decay curves of the emission band at about 612 nm due to the $^5D_0 - {}^7F_2$ transition are shown in Fig. 2(b). The average lifetimes were calculated using (Hasabeldaim and Swart, 2023)

$$\tau = \frac{\int_0^\infty tI(t)dt}{\int_0^\infty I(t)dt} \tag{14}$$

where $I(t)$ is the counts at a given time t. The average lifetime decreased at higher Eu concentrations (0.66 and 1.00 mol%), see Table 2. This behaviour has been observed in many hosts and ascribed to nonradiative energy transfer between Eu^{3+} ions (Van Do et al., 2023; Hien et al., 2021).

Judd-Ofelt parameters, radiative transition probabilities ($A(J, J')$), branching ratios ($ß_{cal}$), and symmetry ratios (R) of the ZnO:Eu^{3+}

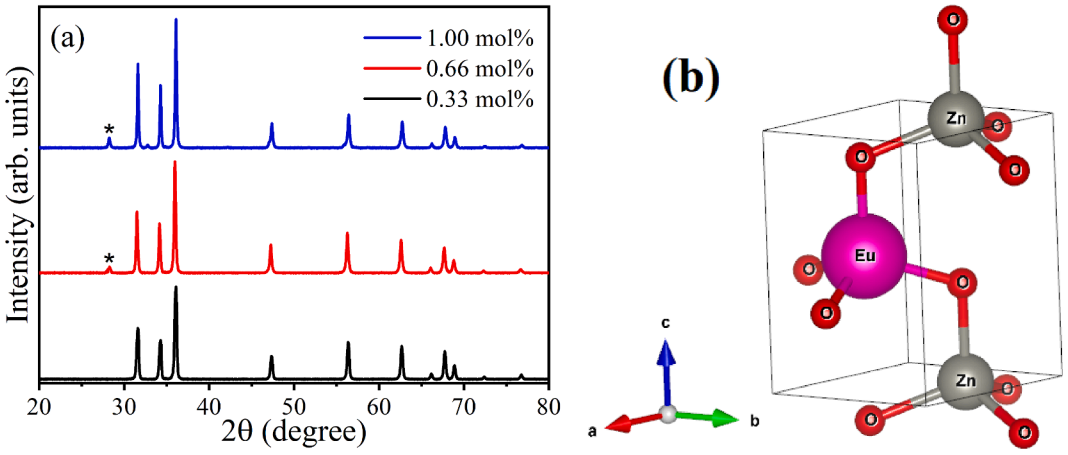

Fig. 1. (a) XRD patterns of ZnO:Eu^{3+} with different doping concentration of Eu and (b) unit cell of the hexagonal wurtzite structure of ZnO:Eu^{3+}.

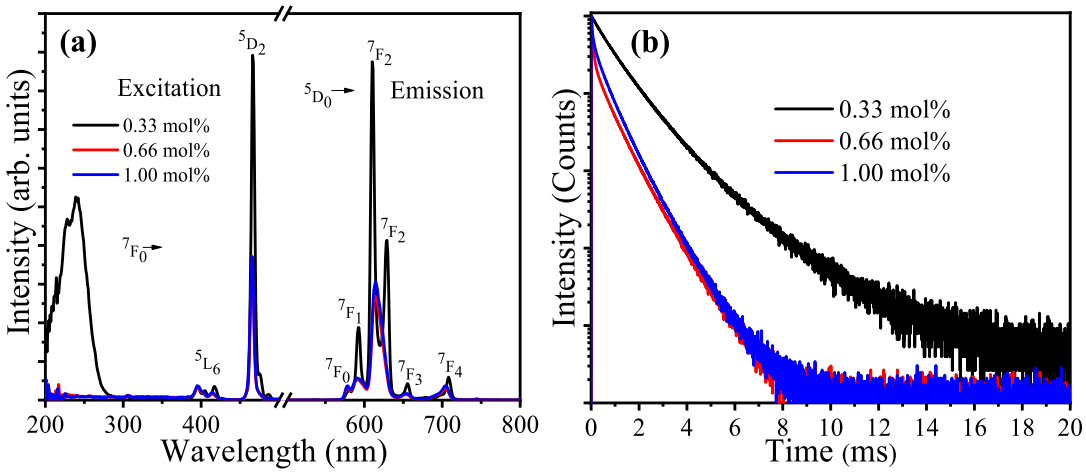

Fig. 2. (a) PL and (b) decay curve of ZnO doped with different Eu^{3+} concentration.

Table 1
Judd–Ofelt parameters (Ω_2, Ω_4), radiative transition probabilities ($A(J, J')$), branching ratios ($ß_{cal}$), and symmetry ratios (R) of the ZnO:Eu^{3+} phosphors.

Eu concentration	Transitions	N	Ω (10^{-20} cm^2)	$A(J, J')(s^{-1})$	$ß_{cal}$ (%)	$\nu(cm^{-1})$	R
0.33 mol%	$^5D_0$-$^7F_1$	2.0021		116	13	16,890	6.025
	$^5D_0$-$^7F_2$	1.9943	8.687	701	81	16,393	
	$^5D_0$-$^7F_4$	1.9729	1.341	48	6	14,124	
0.66 mol%	$^5D_0$-$^7F_1$	2.0021		117	15	16,920	5.150
	$^5D_0$-$^7F_2$	1.9943	7.613	602	76	16,285	
	$^5D_0$-$^7F_4$	1.9729	1.994	72	9	14,206	
1.00 mol%	$^5D_0$-$^7F_1$	2.0021		117	14	16,920	5.382
	$^5D_0$-$^7F_2$	1.9943	7.957	630	76	16,285	
	$^5D_0$-$^7F_4$	1.9729	2.127	77	9	14,183	

Table 2
The radiative lifetimes (τ_r), calculated radiative lifetimes (τ_{cal}), observed lifetimes (τ), quantum efficiencies (η QE), and calculated quantum efficiencies (η_{cal} QE) of the ZnO:Eu^{3+} phosphors.

Eu concentration	τ_r (μs)	τ_{cal} (μs)	τ (μs)	η QE (%)	η_{cal} QE (%)
0.33 mol%	1156	1198	1068	92	89
0.66 mol%	1263	1198	536	42	45
1.00 mol%	1215	1198	561	46	47

phosphors were calculated using the web-based application and listed in Table 1. Fig. 3 depicts the user interface of the web-based application, which can be accessed through the following link, https://sciapps.sci-sim.com/judd_ofelt_analysis_Eu.html. The user can locate and open a photoluminescence spectrum file (csv or txt format) of Eu^{3+} ions via the File button. The PL spectrum will be displayed on the left-side pane, whereas the numerical data will be shown on the right-side pane. The wavelength range for each transition band needs to be inserted in the main table in their respective fields; they can be inserted manually or otherwise by selecting the intended field, hovering over the spectrum using the red vertical line, and double clicking to add the corresponding wavelength. Since the emission facilitated by the $^5D_0 - {}^7F_6$ transition is in most cases weak or not present, the emission bands arising from $^5D_0 - {}^7F_J$ (J = 1, 2, and 4) transitions can only be used. Judd-Ofelt parameters are obtained by a single click on the calculate button. The observed (experimental) lifetime must be inserted to obtain the derived parameters on the secondary table (button).

The application software is also capable of determining the point group symmetry of Eu^{3+} when the number of crystal field splitting for ^7F_J transitions is inserted. However, there are caveats that need to be taken into consideration when identifying the point group symmetries from an emission spectrum: (i) peak overlapping where weak peaks appear as shoulders of the intense peaks, this problem may be overcome by peak fitting; (ii) peak overlap due to overlapping of higher excited state transitions, this could be dealt with by time-gated or low-temperature measurement; (iii) when there are multipole site symmetries, polarized photoluminescence measurement for all transitions is required. The output of the point group symmetry part of the software is based on the results of reference (Binnemans, 2015). There are numerous examples in the literature where the Eu^{3+} ion was used as a spectroscopy probe to determine the point group symmetry by studying the number crystal field splitting of ^7F_J transitions (Tanner, 2013; Blasse and Bril, 1966).

The asymmetric ratio (R) is also computed by the software. It is the ratio between the integrated intensity of the electric and magnetic dipole transitions. It provides information about the degree of distortion from the inversion symmetry.

The value of Ω_2 of the sample containing lower Eu concentration (0.33 mol%) is greater than those with higher Eu content (0.66 and 1.00 mol%), suggesting that Eu occupied a site with higher degree of symmetry distortion for the sample with lower Eu content. The value of Ω_4 increased with increasing Eu concentration, indicating lower rigidity of the environment as the Eu concentration increases. Moreover, since Moura Jr *et al.* (Moura et al., 2016) demonstrated that Ω_4 and Ω_6 are better probes for quantifying Eu^{3+}-ligand bond covalency, the rising value of Ω_4 as the Eu concentration increased indicates that the covalency become greater. Since the intensity parameter (Ω_J) values depends on the ligand symmetry and host structure, their variation as Eu doping increases could be due to the occurrence of mixed phase structure as revealed by XRD analysis. The branching ratio calculated from the radiative transition probabilities $ß_{cal}$ for the $^5D_0 - {}^7F_2$ transition of all samples is greater than 50 %, which indicates a potential laser emission. The asymmetric ratio value of the sample with lower Eu concertation is higher than the samples with greater Eu content, which suggests that the environment is highly distorted. By recalling the XRD results, which confirmed that at lowest Eu concentration the Eu ions occupied a zinc

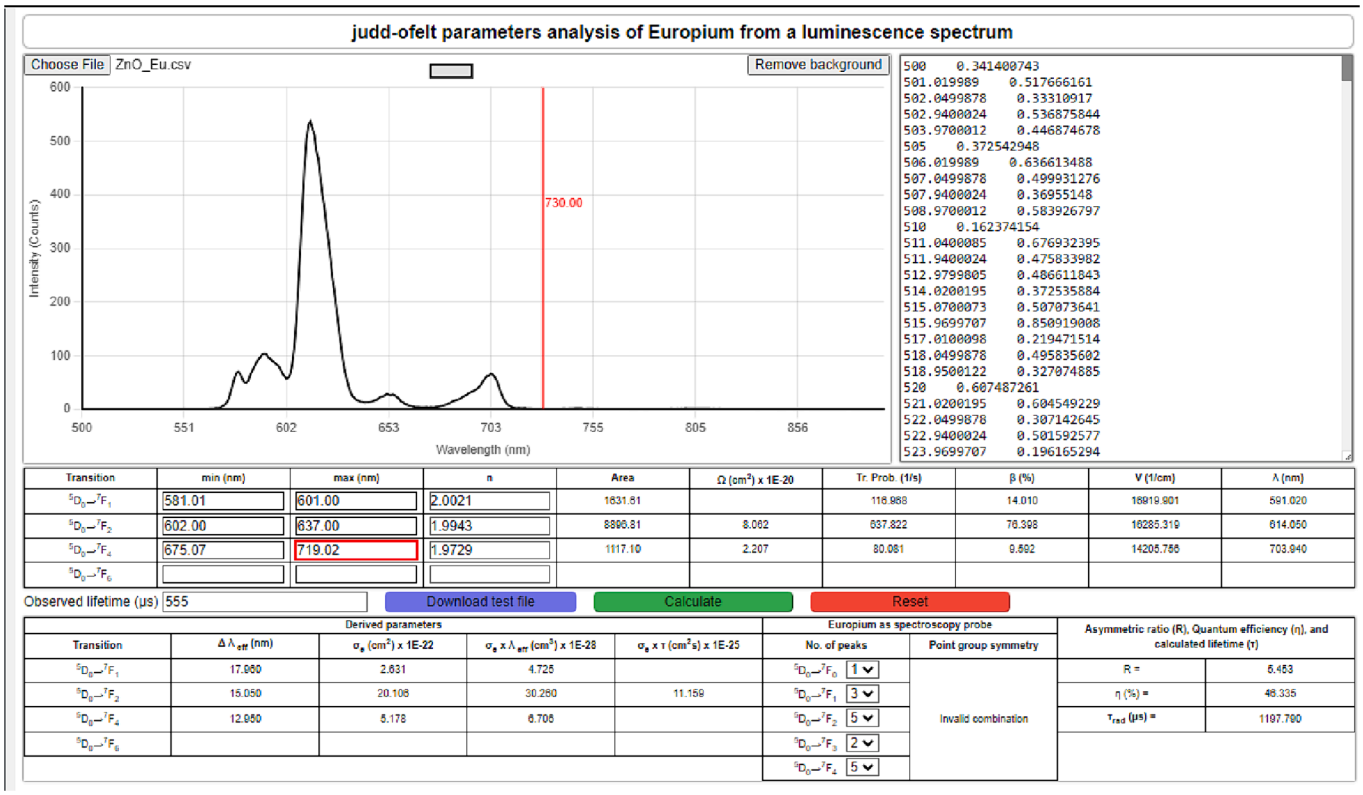

Fig. 3. The web-based user interface of the application for calculating Judd-Ofelt and derived parameters from an emission spectrum of Eu^{3+}.

site of the hexagonal structure, the distorted environment could be due to the charge difference between Eu^{3+} and Zn^{2+} ions which requires a charge compensation process to maintain neutrality.

The lifetimes (radiative, calculated, and observed) and quantum efficiencies (radiative and calculated) were calculated and tabulated in Table 2. The sample with 0.33 mol% of Eu exhibited the highest efficiencies of about 92 % and 89 % for the radiative and calculated quantum efficiencies, respectively. The difference between the radiative and calculated quantum efficiencies is very low, ranging from 1 % to 3 %, indicating acceptable values. The experimental lifetime is always shorter than the calculated or radiative lifetimes, which is associated with the nanoradiative relaxation processes. The nonradiative relaxation rate (W_{NR}) can be calculated by using the following equation (Quang et al., 2019)

$$W_{NR} = \frac{1}{\tau_{exp}} - \frac{1}{\tau_{cal}} \tag{15}$$

The values of W_{NR} were calculated and found to be 102, 1030, and 947 s^{-1} for the samples doped with 0.33, 0.66, and 1.00 mol% of Eu^{3+} ions. The increasing trend with increasing Eu content suggests an increase in the nonradiative transitions between Eu ions as their concentration increases.

The stimulated emission cross-section (σ_e), gain bandwidth (σ_e x λ_{eff}), the effective bandwidth of emission transition (λ_{eff}), and the optical gain (σ_e x τ) results of the samples are given in Table 3. The values were found to be higher for the $^5D_0 - {}^7F_2$ transitions of the sample with 0.33 mol% of Eu^{3+} ions, indicating a potential for low threshold, high optical gain, and band width in the laser medium. It is clear that the Eu site in ZnO plays an important role in the Judd-Ofelt parameters and its derived quantities. When Eu^{3+} ions occupied the Zn site at a lower Eu concentration, the Judd-Ofelt parameters indicated a high degree of symmetry distortion, quantum efficiency, and optical gaining. Unlike at higher Eu concentrations, the derived quantities have drastically reduced, which was attributed to a change in Eu site symmetry and the local chemical environment due to occurrence of mixed phase crystal structure as evident from the XRD results.

Table 3
The effective bandwidth of the emission transitions (Δ_{eff}), stimulated emission cross-sections (σ), gain bandwidths ($\sigma \times \Delta_{eff}$), and optical gains ($\sigma \times \tau$) of the ZnO:$Eu^{3+}$ phosphors.

Eu concentration	Transitions $^5D_0$-	$\Delta\lambda_{eff}$ (nm)	σ_e (10^{-22} cm^2)	$\sigma_e \times \Delta\lambda_{eff}$ (10^{-28} cm^3)	$\sigma_e \times \tau$ (10^{-25} cm^2s)
0.33 mol%	$^7F_1$	5	9	5	69
	$^7F_2$	5	64	32	
	$^7F_4$	6	7	4	
0.66 mol%	$^7F_1$	19	2	5	10
	$^7F_2$	15	19	29	
	$^7F_4$	12	5	6	
1.00 mol%	$^7F_1$	19	2	5	11
	$^7F_2$	15	20	30	
	$^7F_4$	11	6	6	

Generally, the intensity parameter (Ω_2) is about two-fold or more than other materials such as borotellurite glasses (Quang et al., 2019), metal sulfide (Tan et al., 2020; Cuong et al., 2023), and fluoride (Van Do et al., 2023) compounds, whereas Ω_4 is comparable with these materials. This signifies a higher local symmetry distortion around Eu^{3+} ions in the ZnO host. Nevertheless, the quantum efficiency of the sample with lower Eu concentration [ZnO:Eu^{3+} (0.33 mol%)] is comparable with these materials, while the optical gain is even higher. These results demonstrate that ZnO:Eu^{3+} is a potential laser material with superior thermal stability.

5. Manually calculated Judd–Ofelt parameters and the derived quantities

To validate the correctness of the Judd–Ofelt parameters and derived quantities obtained by using the software, the value were calculated manually and presented in Tables 4, 5, and 6. Software-calculated values

Table 4
Judd–Ofelt parameters (Ω_2, Ω_4), radiative transition probabilities (A(J, J')), branching ratios ($ß_{cal}$), and symmetry ratios (R) of the ZnO:Eu^{3+} phosphors.

Eu concentration	Transitions	n	Ω (10^{-20} cm^2)	$A(J, J')$ (s^{-1})	$ß_{cal}$ (%)	ν (cm^{-1})	R
0.33 mol%	$^5D_0$-$^7F_1$	2.0021		116	13	16890	6.0
	$^5D_0$-$^7F_2$	1.9943	8.7	701	81	16393	
	$^5D_0$-$^7F_4$	1.9729	1.3	48	6	14124	
0.66 mol%	$^5D_0$-$^7F_1$	2.0021		117	15	16920	5.2
	$^5D_0$-$^7F_2$	1.9943	7.6	602	76	16285	
	$^5D_0$-$^7F_4$	1.9729	2.0	72	9	14206	
1.00 mol%	$^5D_0$-$^7F_1$	2.0021		117	14	16920	5.4
	$^5D_0$-$^7F_2$	1.9943	8.0	630	76	16285	
	$^5D_0$-$^7F_4$	1.9729	2.1	77	9	14183	

Table 5
The radiative lifetimes (τ_r), calculated radiative lifetimes (τ_{cal}), observed lifetimes (τ), quantum efficiencies (η QE), and calculated quantum efficiencies (η_{cal} QE) of the ZnO:Eu^{3+} phosphors.

Eu concentration	τ_r (μs)	τ_{cal} (μs)	τ (μs)	η QE (%)	η_{cal} QE (%)
0.33 mol%	1156	1198	1068	92	89
0.66 mol%	1263	1198	536	42	45
1.00 mol%	1215	1198	561	46	47

Table 6
The effective bandwidth of the emission transitions (Δ_{eff}), stimulated emission cross-sections (σ), gain bandwidths (σ x Δ_{eff}), and optical gains (σ x τ) of the ZnO:Eu^{3+} phosphors.

Eu concentration	Transitions $^5D_0$-	$\Delta\lambda_{eff}$ (nm)	σ_e (10^{-22} cm^2)	σ_e x $\Delta\lambda_{eff}$ (10^{-28} cm^3)	σ_e x τ (10^{-25} cm^2s)
0.33 mol%	$^7F_1$	5	9	5	69
	$^7F_2$	5	64	32	
	$^7F_4$	6	7	4	
0.66 mol%	$^7F_1$	19	2	5	10
	$^7F_2$	15	19	29	
	$^7F_4$	12	5	6	
1.00 mol%	$^7F_1$	19	2	5	11
	$^7F_2$	15	20	30	
	$^7F_4$	11	6	6	

match well with the manually calculated values, proving that the software yields correct and reliable calculations. OriginLAB software was used for calculating the integrated photoluminescence from the Eu^{3+} spectrum, the integration range was the same as the ranges used for calculating the values by using the software.

6. Conclusion

A web-based application for calculating Judd-Ofelt intensity and derived parameters from emission spectra of Eu^{3+} doped materials was successfully developed using the JavaScript programming language. It is accessible at https://sciapps.sci-sim.com/judd_ofelt_analysis_Eu.html and can be used free of charge. Three ZnO doped with different amounts of Eu^{3+} ions were synthesized and used as testing samples. Upon thorough testing, the output results indicated that the application is reliable and time efficient. Furthermore, the results demonstrated that ZnO doped with the lowest amount of Eu^{3+} ions (0.33 mol%) is a potential laser material. This application is a useful computational tool in the field of experimental luminescent rare earth ions, to quickly assess the radiative properties of and the chemical environment around Eu^{3+} ions in a host material.

CRediT authorship contribution statement

E.H.H. Hasabeldaim: Software, Methodology, Investigation, Conceptualization. **H.C. Swart:** Writing – review & editing, Resources, Funding acquisition. **R.E. Kroon:** Writing – review & editing, Supervision, Project administration.

Declaration of competing interest

The authors declare that they have no known competing financial interests or personal relationships that could have appeared to influence the work reported in this paper.

Data availability

Data will be made available on request.

Acknowledgement

This work is supported by the South African Research Chairs Initiative of the Department of Science and Technology (84415) and National Research Foundation of South Africa.

References

M. P. Hehlen, "Rare Earth Level and Intensity Calculations, (n.d.). http://www.lanl.gov/projects/feynman-center/deploying-innovation/intellectual-property/ software-tools/relic/index.php.

Babu, S.S., Babu, P., Jayasankar, C.K., Sievers, W., Tröster, T., Wortmann, G., 2007. Optical absorption and photoluminescence studies of Eu3+-doped phosphate and fluorophosphate glasses. J. Lumin. 126, 109–120. https://doi.org/10.1016/j.jlumin.2006.05.010.

Binnemans, K., 2015. Interpretation of europium (III) spectra. Coord. Chem. Rev. 295, 1–45. https://doi.org/10.1016/j.ccr.2015.02.015.

Blasse, G., Bril, A., 1966. On the Eu3+ fluorescence in mixed metal oxides. V. The Eu3+ fluorescence in the rocksalt lattice. J. Chem. Phys. 45 (9), 3327–3332. https://doi.org/10.1063/1.1728110.

Brik, M.G., Antic, Z.M., Vukovic, K., Dramicanin, M.D., 2015. Judd-Ofelt analysis of Eu3 + emission in TiO2 anatase nanoparticles. Mater. Trans. 56, 1416–1418. https://doi.org/10.2320/matertrans.MA201566.

Cantelar, E., Sanz-García, J.A., Sanz-Martin, A., Santiuste, J.E.M., Cussó, F., 2020. Structural, photoluminescent properties and Judd-Ofelt analysis of Eu3+-activated CaF2 nanocubes. J. Alloys Compd. 813, 152194 https://doi.org/10.1016/j.jallcom.2019.152194.

Carnall, W.T., Goodman, G.L., Rajnak, K., Rana, R.S., 1989. A systematic analysis of the spectra of the lanthanides doped into single crystal LaF_3. J. Chem. Phys. 90, 3443–3457. https://doi.org/10.1063/1.455853.

Ćirić, A., Stojadinović, S., Sekulić, M., Dramićanin, M.D., 2019. JOES: An application software for Judd-Ofelt analysis from Eu3+ emission spectra. J. Lumin. 205, 351–356. https://doi.org/10.1016/j.jlumin.2018.09.048.

Cuong, K.C., Thuy, N.T.M., Fan, X., Hao, P.V., Quynh, L.K., Huong, T.T.T., Kien, N.T., Van, N.T.K., Hien, N.T., Dung, L.N., Ca, N.X., 2023. Optical properties, Judd-Ofelt analysis and energy transfer processes of Eu3+ doped ZnS quantum dots. Chem. Phys. Lett. 832, 140896 https://doi.org/10.1016/j.cplett.2023.140896.

Danmallam, I.M., Ghoshal, S.K., Ariffin, R., Jupri, S.A., Sharma, S., Bulus, I., 2019. Judd-Ofelt evaluation of europium ion transition enhancement in phosphate glass. Optik 196, 163197. https://doi.org/10.1016/j.ijleo.2019.163197.

Dutra, J.D.L., Bispo, T.D., Freire, R.O., 2014. LUMPAC lanthanide luminescence software: efficient and user friendly. J. Comput. Chem. 35, 772–775. https://doi.org/10.1002/jcc.23542.

Gökçe, M., Şentürk, U., Uslu, D.K., Burgaz, G., Şahin, Y., Gökçe, A.G., 2017. Investigation of europium concentration dependence on the luminescent properties of borogermanate glasses. J. Lumin. 192, 263–268. https://doi.org/10.1016/j.jlumin.2017.06.041.

C. Görller-Walrand, K. Binnemans, "Chapter 167 spectral intensities of f-f transitions, Handb" *Phys. Chem. Rare Earths* (1998) 101–264. doi: 10.1016/S0168-1273(98)25006-9.

E. H. H. Hasabeldaim, H. C. Swart, R. E. and Kroon, "Luminescence and stability of Tb doped CaF_2 nanoparticles." *RSC Adv.* **13(8)** (2023) 5353-5366. 10.1039/D2RA07897J.

Hasabeldaim, E.H.H., Ntwaeaborwa, O.M., Kroon, R.E., Coetsee, E., Swart, H.C., 2019. Photoluminescence and cathodoluminescence of spin coated ZnO films with different concentration of Eu3+ ions. Vacuum 169, 108889. https://doi.org/10.1016/j.vacuum.2019.108889.

Hasabeldaim, E., Ntwaeaborwa, O.M., Kroon, R.E., Swart, H.C., 2019. Structural, optical and photoluminescence properties of Eu doped ZnO thin films prepared by spin coating. J. Mol. Struct. 1192, 105–114. https://doi.org/10.1016/j.molstruc.2019.04.128.

Hasabeldaim, E.H.H., Ntwaeaborwa, O.M., Kroon, R.E., Coetsee-Hugo, E., Swart, H.C., 2020. Pulsed laser deposition of a ZnO: Eu3+ thin film: Study of the luminescence and surface state under electron beam irradiation. Appl. Surf. Sci. 502, 144281 https://doi.org/10.1016/j.apsusc.2019.144281.

Hehlen, M.P., Brik, M.G., Krämer, K.W., 2013. 50th anniversary of the Judd-Ofelt theory: an experimentalist's view of the formalism and its application. J. Lumin. 136, 221–239. https://doi.org/10.1016/j.jlumin.2012.10.035.

Hien, N.T., Yu, Y.Y., Park, K.C., Ca, N.X., Chi, T.T.K., Hien, B.T.T., Thanh, L.D., Do, P.V., Tan, P.M., Ha, P.T.T., 2021. Influence of Eu doping on the structural and optical properties of Zn1-xEuxSe quantum dots. J. Phys. Chem. Solids 148, 109729. https://doi.org/10.1016/j.jpcs.2020.109729.

Ilhan, M., Ekmekçi, M.K., Keskin, I.C., 2021. Judd–Ofelt parameters and X-ray irradiation results of MNb2O6: Eu3+(M= Sr, Cd, Ni) phosphors synthesized via a molten salt method. RSC Adv. 11 (18), 10451–10462. https://doi.org/10.1039/d0ra10834k.

Judd, B.R., 1962. Optical absorption intensities of rare-earth ions. Phys. Rev. 127 (3), 750. https://doi.org/10.1103/PhysRev.127.750.

Korotkov, A.S., Atuchin, V.V., 2008. Prediction of refractive index of inorganic compound by chemical formula. Opt. Commun. 281 (8), 2132–2138. https://doi.org/10.1016/j.optcom.2007.12.030.

Kumar, R.A., Hata, S., Ikeda, K.I., Gopchandran, K.G., 2016. Organic mediated synthesis of highly luminescent Li+ ion compensated Gd2O3:Eu3+ nanophosphors and their Judd-Ofelt analysis. RSC Adv. 6 (71), 67295–67307. https://doi.org/10.1039/C5RA26095G.

L. ačanin, S.R. Luki, D.M. Petrovi, M. Nikoli, M.D. Dramićanin, "Judd–Ofelt analysis of luminescence emission from $Zn_2SiO_4:Eu^{3+}$ nanoparticles obtained by a polymer assisted sol–gel method" *Phys. B Condens. Matter* **406** (2011) 2319–2322. https://doi.org/10.1016/j.physb.2011.03.068.

G. Liu, and B. Jacquier, eds., 2006. *Spectroscopic properties of rare earths in optical materials* (Vol. 83). Springer Science & Business Media.

Moura Jr, R.T., Neto, A.N.C., Longo, R.L., Malta, O.L., 2016. On the calculation and interpretation of covalency in the intensity parameters of 4f–4f transitions in Eu3+ complexes based on the chemical bond overlap polarizability. J. Lumin. 170, 420–430. https://doi.org/10.1016/j.jlumin.2015.08.016.

Ofelt, G.S., 1962. Intensities of crystal spectra of rare-earth ions. J. Chem. Phys. 37 (3), 511–520. https://doi.org/10.1063/1.1701366.

Quang, V.X., Van Tuyen, H., Ngoc, T., Tuyen, V.P., Thanh, L.D., Ca, N.X., Hien, N.T., 2019. Structure, optical properties and energy transfer in potassium-alumino-borotellurite glasses doped with Eu3+ ions. J. Lumin. 216, 116748 https://doi.org/10.1016/j.jlumin.2019.116748.

Saraf, R., Shivakumara, C., Behera, S., Dhananjaya, N., Nagabhushana, H., 2015. Synthesis of Eu3+-activated BiOF and BiOBr phosphors: photoluminescence, Judd-Ofelt analysis and photocatalytic properties. RSC Adv. 5 (12), 9241–9254. https://doi.org/10.1039/C4RA16645K.

C. Shivakumara, and R. Saraf "Eu^{3+}-activated $SrMoO_4$ phosphors for white LEDs applications: Synthesis and structural characterization." Opt. Mater. **42** (2015) 178-186. https://doi.org/10.1016/j.optmat.2015.01.006.

Steckl, A.J., Zavada, J.M., 1999. Photonic applications of rare-earth-doped materials. MRS Bull. 24 (9), 16–20. https://doi.org/10.1557/S0883769400053008.

Tan, P.M., Ca, N.X., Hien, N.T., Van, H.T., Do, P.V., Thanh, L.D., Yen, V.H., Tuyen, V.P., Peng, Y., Tho, P.T., 2020. New insights on the energy transfer mechanisms of Eu-doped CdS quantum dots. Phys. Chem. Chem. Phys. 22 (11), 6266–6274. https://doi.org/10.1039/C9CP06778G.

Tanner, P.A., 2013. Some misconceptions concerning the electronic spectra of tri-positive europium and cerium. Chem. Soc. Rev. 42 (12), 5090–5101. https://doi.org/10.1039/C3CS60033E.

Van Do, P., Ca, N.X., Thanh, L.D., Quan, D.D., Hung, N.M., Du, P.T., Huong, N.T., Anh, D. T., 2023. NaGdF4:Eu3+ nanocrystalline: an in-depth study of energy transfer processes and Judd-Ofelt analysis using the luminescence excitation spectrum. Phys. Chem. Chem. Phys. 25 (41), 28296–28308. https://doi.org/10.1039/d3cp02458j.

Werts, M.H.V., Jukes, R.T.F., Verhoeven, J.W., 2002. The emission spectrum and the radiative lifetime of Eu3+ in luminescent lanthanide complexes. Phys. Chem. Chem. Phys. 4, 1542–1548. https://doi.org/10.1039/b107770h.

Werts, M.H., Jukes, R.T., Verhoeven, J.W., 2002. The emission spectrum and the radiative lifetime of Eu3+ in luminescent lanthanide complexes. Phys. Chem. Chem. Phys. 4 (9), 1542–1548. https://doi.org/10.1039/b107770h.

Yu, C., Zhang, X., Li, X., Zhang, J., Xu, S., Zhang, X., Zhang, Y., Wang, X., Wang, L., Sui, G., Chen, B., 2019. Determination of Judd-Ofelt parameters for Eu3+-doped alkali borate glasses. MRS Bull. 120, 110590 https://doi.org/10.1016/j.materresbull.2019.110590.